

Inhibition of EZH2 exerts antitumorigenic effects in renal cell carcinoma via LATS1

Seong Hwi Hong¹, Hyun Ji Hwang^{1,2}, Da Hyeon Son^{1,2}, Eun Song Kim^{1,2}, Sung Yul Park¹ and Young Eun Yoon¹ 

¹ Department of Urology, Hanyang University College of Medicine, Seoul, Korea

² Department of Translational Medicine, Hanyang University Graduate School of Biomedical Science & Engineering, Seoul, Korea

Keywords

EZH2; Hippo pathway; LATS1; renal cell carcinoma; tazemetostat

Correspondence

Y. E. Yoon, Department of Urology, Hanyang University College of Medicine, Seoul, Republic of Korea
 Tel: +82 2 2290 8593
 Fax: +82 2 2299 2186
 E-mail: urologistyoonyoon@hanyang.ac.kr

(Received 17 July 2022, revised 1 February 2023, accepted 20 February 2023)

doi:10.1002/2211-5463.13579

Edited by Ivana Novak

The most common type of kidney cancer in adults is renal cell carcinoma (RCC), which accounts for approximately 90% of cases. RCC is a variant disease with numerous subtypes; the most common subtype is clear cell RCC (ccRCC, 75%), followed by papillary RCC (pRCC, 10%) and chromophobe RCC (chRCC, 5%). To identify a genetic target for all subtypes, we analyzed The Cancer Genome Atlas (TCGA) databases of ccRCC, pRCC, and chromophobe RCC. Enhancer of zeste homolog 2 (EZH2), which encodes a methyltransferase, was observed to be significantly upregulated in tumors. The EZH2 inhibitor tazemetostat induced anticancer effects in RCC cells. TCGA analysis revealed that large tumor suppressor kinase 1 (LATS1), a key tumor suppressor of the Hippo pathway, was significantly downregulated in tumors; the expression of LATS1 was increased by tazemetostat. Through additional experiments, we confirmed that LATS1 plays a crucial role in EZH2 inhibition and has a negative association with EZH2. Therefore, we suggest that epigenetic control could be a novel therapeutic strategy for three subtypes of RCC.

Although kidney cancer comprises only 2–3% of all cancers worldwide [1], it is the 10th most frequent cancer among men and women. The most common type of kidney cancer in adults is renal cell carcinoma (RCC), accounting for approximately 90% of cases. RCC is a variant disease with numerous subtypes; the most common subtype is clear cell RCC (ccRCC, 75%), followed by papillary RCC (pRCC, 10%) and chromophobe RCC (chRCC, 5%) [2]. Most kidney cancer research is limited to ccRCC to account for the largest portion of RCC cases. In clinical practice, treatment methods for non-ccRCC are not standardized and are still considered in clinical trials according

to the National Cancer Network guidelines. Therefore, it is important to discover new therapeutic targets that can encompass multiple subtypes of RCC.

Enhancer of zeste homolog 2 (EZH2) is a methyltransferase that catalyzes trimethylation of H3K27 (histone 3 lysine 27) as a major factor of polycomb repressive complex 2 involved in epigenetic gene silencing [3,4]. It is known to regulate the expression of genes involved in cell differentiation and development and to cause cancer by inhibiting the transcription of tumor suppressor genes [5]. It is overexpressed in various cancers, including breast cancer [6], glioblastoma [7], bladder cancer [8], liver cancer [9], and lung cancer

Abbreviations

ChIP, chromatin immunoprecipitation; ccRCC, clear cell RCC; EZH2, enhancer of zeste homolog 2; FITC, fluorescein isothiocyanate; H3K27me3, trimethylation of histone 3 lysine 27; IHC, immunohistochemistry; LATS1, large tumor suppressor kinase 1; MSigDB, molecular signatures database; PI, propidium iodide; pRCC, papillary RCC; RCC, renal cell carcinoma; TCGA, The Cancer Genome Atlas; TKIs, tyrosine kinase inhibitors; YAP1, yes-associated protein 1.

[10,11]. Currently, tazemetostat, a selective inhibitor of EZH2, is undergoing clinical trials in urinary cancers including bladder cancer (NCT04019327) and prostate cancer (NCT04019327). However, although a recent study reported the potential of EZH2 as a prognostic marker related to the survival rate of RCC patients [12], the effect and underlying mechanism of tazemetostat are unknown in RCC.

The Hippo pathway is not only involved in regulating the size of an animal's organs through cell growth and death but also plays an important role in regulating metabolic homeostasis [13]. LATS1 is a key component of the Hippo pathway [14]. When the Hippo pathway is turned on, LATS1 induces the degradation of YAP/TAZ, thereby maintaining a state in which cancer cell growth and metastasis are inhibited. However, turning off the Hippo pathway inhibits the degradation of YAP/TAZ, which then enters the nucleus and acts as a transcription cofactor that promotes the transcription of genes, especially oncogenes, leading to cancer growth and metastasis [14,15].

In this study, we discovered key factors that can target multiple subtypes of RCC and ccRCC. We aimed to assess the effects of an EZH2 inhibitor on the Hippo pathway to better understand epigenetic modulators and identify a common drug target for the major RCC subtypes.

Materials and methods

Cell culture

The human ccRCC cell line Caki-1 and the pRCC cell line ACHN were purchased from Korean Cell Line Bank (Seoul, South Korea). The immortalized human chRCC cell line UOK-276 was kindly provided by W. Marston Linehan (National Cancer Institute, Maryland, USA). All cell lines were maintained in RPMI-1640 or Dulbecco's modified Eagle medium (Sigma-Aldrich, St. Louis, Missouri, USA) supplemented with 10% fetal bovine serum (FBS; Sigma-Aldrich) and 1× antibiotic-antimycotic (Thermo Fisher, Waltham, Massachusetts, USA). All cells were cultured in an incubator designed to maintain a constant temperature and high humidity for the growth of cells under 5% CO₂ atmosphere.

Cell viability

Cell viability was measured using EZ-CYTOX (DoGenBio, #EZ-1000, Seoul, Korea). RCC cells were grown to 50% confluency in 96-well plates (SPL, Kyonggi-do, South Korea) and treated with 0 to 100 μM tazemetostat for 24 h at 37 °C. Following incubation, 10 μL of EZ-CYTOX solution was added to each well. Absorbance at a wavelength

of 450 nm was determined by a microplate reader (BIO-RAD, #1681130, Hercules, California, USA). The cell viability rates were calculated, and graphs were generated. The cell viability was evaluated based on the treated group versus the untreated group results.

RNA extraction and reverse transcription PCR

Using TRIzol reagent, total RNA was extracted and reverse transcribed using an AccuPower RT PreMix kit (Bioneer Daejeon, South Korea). For qRT-PCR analysis, cDNAs were amplified with LightCycler® 480 SYBR Green I Master Mix (Roche, Basel, Switzerland). Using a LightCycler® 480 II PCR system (Roche), the cycle threshold value (Ct value) and the exponential amplification time of the PCR product were monitored in real time. cDNAs were amplified using the following primers: RT_*GAPDH*_forward, 5'-GAG TCA ACG GAT TTG GTC GT; RT_*GAPDH*_reverse, 3'-TGG AAG ATG GTG ATG GGA TT; RT_*LATS1*_forward, 5'-CTC CAC CAC CTC TCA ACA CT; and RT_*LATS1*_reverse, 3'-CGA TTC ACA GTG CCA GCA G. PCR conditions consisted of a predenaturation step of 95 °C for 5 min, followed by 60 cycles of 95 °C for 1 min, 60 °C for 1 min, and 72 °C for 1 min, with a final extension of 72 °C for 10 min.

Apoptosis assay

The apoptosis rate was assessed using the annexin V-fluorescein isothiocyanate (FITC) apoptosis detection kit (BD Biosciences, #556547, Franklin Lakes, New Jersey, USA). Cells were transfected with siLATS1 and treated with various concentrations of tazemetostat for a further period of 24 h. For each sample, the collected supernatant and trypsinized cells were rinsed in Dulbecco's phosphate-buffered saline and suspended in 1× binding buffer at a concentration of 1 × 10⁶ cells/mL. Then, 5 μL FITC-conjugated annexin V and 2 μL propidium iodide (PI) were added to 100 μL containing 1 × 10⁵ cells and incubated for 15 min at room temperature in the dark. After incubation, 400 μL binding buffer (1×) was added to each tube, and the cells were analyzed using a FACSCanto flow cytometer (BD Biosciences).

Western blot analysis

Cells were lysed with protein lysis radio-immunoprecipitation assay buffer and briefly sonicated for complete lysis of protein. Cell lysates were boiled with 4× sample buffer, and 30 μg of each protein was separated by sodium dodecyl sulfate-polyacrylamide gel electrophoresis. For the quantitation of protein, the lysate was measured by bicinchoninic acid assay. Antibodies against EZH2 (1 : 1000, #195409, Abcam, Cambridge, UK), LATS1 (1 : 1000, Cell Signaling Technology, #3477S, Danvers,

Massachusetts, USA), yes-associated protein 1 (YAP1; 1 : 1000, Cell Signaling Technology, #14074S), H3K27me3 (1 : 500, Abcam, #195477), histone H3 (1 : 1000, Abcam, #ab1791), beta-actin (1 : 1000, GeneTex, #GTX109639, Irvine, California, USA) were purchased from the indicated companies. We analyzed the protein expression using ChemiDoc XRS+ with IMAGE LAB software and quantitated the band using IMAGEJ software (version 1.53t) [16].

Chromatin immunoprecipitation assay

For the chromatin immunoprecipitation (ChIP) assay, we used Pierce™ Agarose ChIP kit (Thermo Fisher, #26156). ChIP assays were performed according to instructions from the manufacturer. Briefly, 50 µg DNA fragmented to 200–500 bp in size by enzymatic digestion was precleared with protein A magnetic beads. The precleared DNA was immunoprecipitated with EZH2 (1 µL, Abcam, #195409) and H3K27me3 (1 µL, Abcam, #195477). After this, DNA extraction was performed for chromatin fragments, and qPCR was performed on the DNA bound to each target protein using LightCycler 480 II (Roche). Immunoglobulin G experiments as the negative control were conducted for all samples. The qPCR results were calculated as IP/1% input as follows: $(IP - IgG)/(Input - IgG)$. The following specific primers were used for ChIP-qPCR of chromatin fragments: ChIP_LATS1 promoter_forward, CGC TCA CGA ACG ATC AGA; ChIP_LATS1 promoter_reverse, GAC CTG GCT CTC CCC TTA AC.

Wound healing assay

Cells were seeded to an even cell density and grown to 80% confluency in 6-well cell culture plates. After overnight incubation in a serum-free medium, cell layers were scratched with sterile yellow tips. The cell images for the width of the initial gap (0 h) and the residual gap at 16 or 24 h after wounding were captured and measured using an optical microscope at 40× magnification (Nikon, Eclipse TS100, Tokyo, Japan).

Invasion assay

For the invasion assay, cell motility was measured using a Boyden chamber-like design (BD Biosciences). To coat the upper surface of the transwell chamber, 100 µL Matrigel (0.3 mg·mL⁻¹, BD Biosciences) was used. After coating for 3 h at 37 °C, the remaining supernatant was removed, 1 × 10⁶/500 µL cell suspension was placed in the top chamber, and the chambers were placed in a 24-well plate. As a chemoattractant, 700 µL 20% FBS medium was incubated under the chamber overnight. The next day, the membrane of the chamber was stained using 0.4% crystal violet. The images of the invaded cells were captured using a microscope at 40× magnification (Nikon, Eclipse TS100), and the cell numbers were quantitated in image fields.

TCGA data analysis

To investigate *EZH2* and *LATS1* levels in a larger RCC cohort, we analyzed RNA-seq-based gene expression profiling data from The Cancer Genome Atlas (TCGA) RCC project (KIRC-ccRCC, KIRP-pRCC, and KICH-chRCC) [17–19]. A log₂ transformation for raw data of RNA-seq was identically applied. Then, the fold change for expression of the tumor and the normal tissues (healthy kidney tissue) was compared. The Molecular Signatures Database (MSigDB) is one of the most widely used and comprehensive databases of gene sets for performing gene set enrichment analysis. Anyone is possible to direct analysis on the website (<https://www.gsea-msigdb.org>), and more detailed information for MSigDB can be found in this article [20].

Immunohistochemistry

Formalin-fixed paraffin-embedded tissue samples were prepared using one T1 stage and two T3 stage tumor tissues obtained from three randomly selected patients. The paraffin-embedded tissues of RCC patients were first cut into <3-mm-thick sections to prepare the tissue slides. The slide of each section was deparaffinized with xylene and hydrated by alcohol. To protect disruption after 3,3'-diaminobenzidine development by endogenous peroxidase activity, the slide was washed in 0.6% H₂O₂ in methanol for 15 min. Then, the slides were treated with 0.1% Triton-X 100, washed three times with phosphate-buffered saline, and blocked with 10% goat serum. To examine the expressions of EZH2 (1 : 500, Abcam, #195409) and LATS1 (1 : 500, Cell Signaling Technology, #3477S), the slides were treated with a corresponding primary antibody overnight at 4 °C, and the next day, it was incubated with secondary antibody at room temperature. The slide was chromogenic reacted using the 3,3'-diaminobenzidine kit (Vector Laboratories, Burlingame, California, USA) and counterstained by hematoxylin and bluing solution. A coverslip was mounted on the slide and observed under an optical microscope (Leica DM4000B, Leica Microsystems, Wetzlar, Germany) at 200× magnification. Using software LEICA APPLICATION SUITE version 4.1.0, the stained area relative to the area of total tissue was calculated and quantified as a percentage.

Transient transfections

The next day after seeding RCC cells in 6-well plates, they were transiently transfected using 100 nm siRNA (Bioneer, #9113, Daejeon, South Korea) and Lipofectamine 2000 reagent (Thermo Fisher). After overnight incubation, Opti-MEM was replaced with an antibiotic-free growth medium.

Statistical analyses

All experiments were performed in triplicate, and all data were analyzed in triplicate. The results are indicated as the

means \pm standard deviation. Statistical calculations and comparisons were completed using a *t*-test or one-way analysis of variance and Tukey's *post hoc* test with GRAPHPAD PRISM 8.0 (GraphPad, San Diego, California, USA). A *P*-value <0.05 was considered statistically significant.

Ethics

Institutional Review Board Statement: The study was conducted according to the guidelines of the Declaration of Helsinki and approved by the Institutional Review Board of Hanyang University Hospital (protocol code number #HYUH 2019-12-002-007, 06-DEC-2021). Written informed consent was obtained from all subjects involved in the study.

Results

Epigenetic enzyme *EZH2* is overexpressed in three RCC subtype cohorts and *EZH2* inhibition by small-molecule tazemetostat induces antitumorogenic effects in RCC cells

The Cancer Genome Atlas database was analyzed to find targets for ccRCC, pRCC, and chRCC. Among the genes with more than 1.5-fold change in common in the three RCCs, 1850 genes were downregulated and 156 genes were upregulated in tumor tissue compared with nontumor tissue. In RCCs, 156 upregulated genes were classified into eight categories according to their role using gene family categorization provided by the MSigDB in gene set enrichment analysis (<https://www.gsea-msigdb.org>) (Fig. S1A). Among the eight categories, we tried to find a main target of RCCs in transcription factors because it can directly affect the transcription of other genes. Recently, because interest in epigenetic regulators for cancer treatment is increasing, *EZH2* as the only epigenetic enzyme was selected in 23 transcription factors that satisfy all conditions. We observed that *EZH2* was significantly increased in tumors compared with nontumor (Fig. S1B). Because tazemetostat is a potent inhibitor of *EZH2* [21], its sensitivities to ccRCC (Caki-1), pRCC (ACHN), and chRCC (UOK-276) cell lines were assessed. To investigate the role of *EZH2* in cell proliferation, we measured cell viability using a colorimetric assay, which is an MTT-based assay. Tazemetostat dose-dependently reduced the growth rate of all three cell lines (Fig. 1A). Consistent with this result, in scratch wound healing and invasion experiments, tazemetostat diminished wound healing capability and invasion in Caki-1, ACHN, and UOK-276 cells (0, 5, 10, 25 μM : 1.9, 35.4, 43.7, and 78.5% for Caki-1, 16.9, 83.7, 91.7, and

94.9% for ACHN, and 1.8, 47.2, 57.6, and 73.6% for UOK-276) (Fig. 1B,C, Fig. S2A). To further study the antitumorogenic effect of tazemetostat, we also examined apoptosis and found increased apoptosis effects in RCC cell lines (0, 5, 10, 25 μM : 1.4, 2.1, 3.2, and 9.1% for Caki-1; 1.8, 2.8, 3.3, and 10.1% for ACHN; and 2.3, 5.1, 7.3, and 12.9% for UOK-276, respectively) (Fig. 1D and Fig. S2B). The cumulative results reveal that *EZH2* could be a remedial strategic target in three major types of RCC and that the inactivation of *EZH2* by tazemetostat has anticancer effects in RCC cell lines.

LATS1 of the Hippo pathway is the main target of *EZH2* inhibition in RCCs

Since the main role of overexpressed *EZH2* in cancer is to suppress the expression of tumor suppressor genes [22,23], we predicted that the expression of the tumor suppressor gene can be recovered by *EZH2* inactivation in RCCs. To find out what tumor suppressors are increased by tazemetostat, we focused on genes that were downregulated in tumor compared with nontumor tissues through TCGA analysis (Fig. 2A). We observed that the large tumor suppressor kinase 1 (*LATS1*), a key tumor suppressive gene of the hippo pathway, was commonly downregulated in the three subtypes of RCC (mean value of NT and T: 8.97 and 8.31 for ccRCC; 8.45 and 7.31 for pRCC, and 8.51 and 7.58 for chRCC) (Fig. 2B). Tazemetostat treatment induced a decrease in global levels of trimethylation of histone 3 lysine 27 (H3K27me3) (0, 5, 10, 25 μM for H3K27me3: 100, 64.7, 47.9, and 43.6% for Caki-1, 100, 23.2, 23.4, and 23.6% for ACHN, and 100, 99.6, 51.6, and 48.1% for UOK-276), an increase in *LATS1* expression (0, 5, 10, 25 μM for *LATS1*: 100, 584.9, 920.2, and 1064% for Caki-1, 100, 177.9, 292.8 and 940.6% for ACHN, and 100, 405.4, 627.1, and 868.6% for UOK-276), and a decrease in *YAP1* expression (0, 5, 10, 25 μM for *YAP1*: 100, 73.3, 66, and 54.8% for Caki-1, 100, 91.6, 89.2, and 47.5% for ACHN, and 100, 82.6, 69.4, and 43.3% for UOK-276), known as a negative downstream target of *LATS1* in the hippo pathway, in a dose-dependent manner (Fig. 2C,D, and Fig. S2C).

Loss of *LATS1* interferes with anticancer effects by *EZH2* inactivation

To further investigate whether *EZH2* is essential for the suppression of *LATS1*, we performed a loss-of-function study by knockdown of *LATS1* cells using siRNA in Caki-1, ACHN, and UOK-276 RCC cells (Fig. S3A). As shown in Fig. 3A and Fig. S3B,

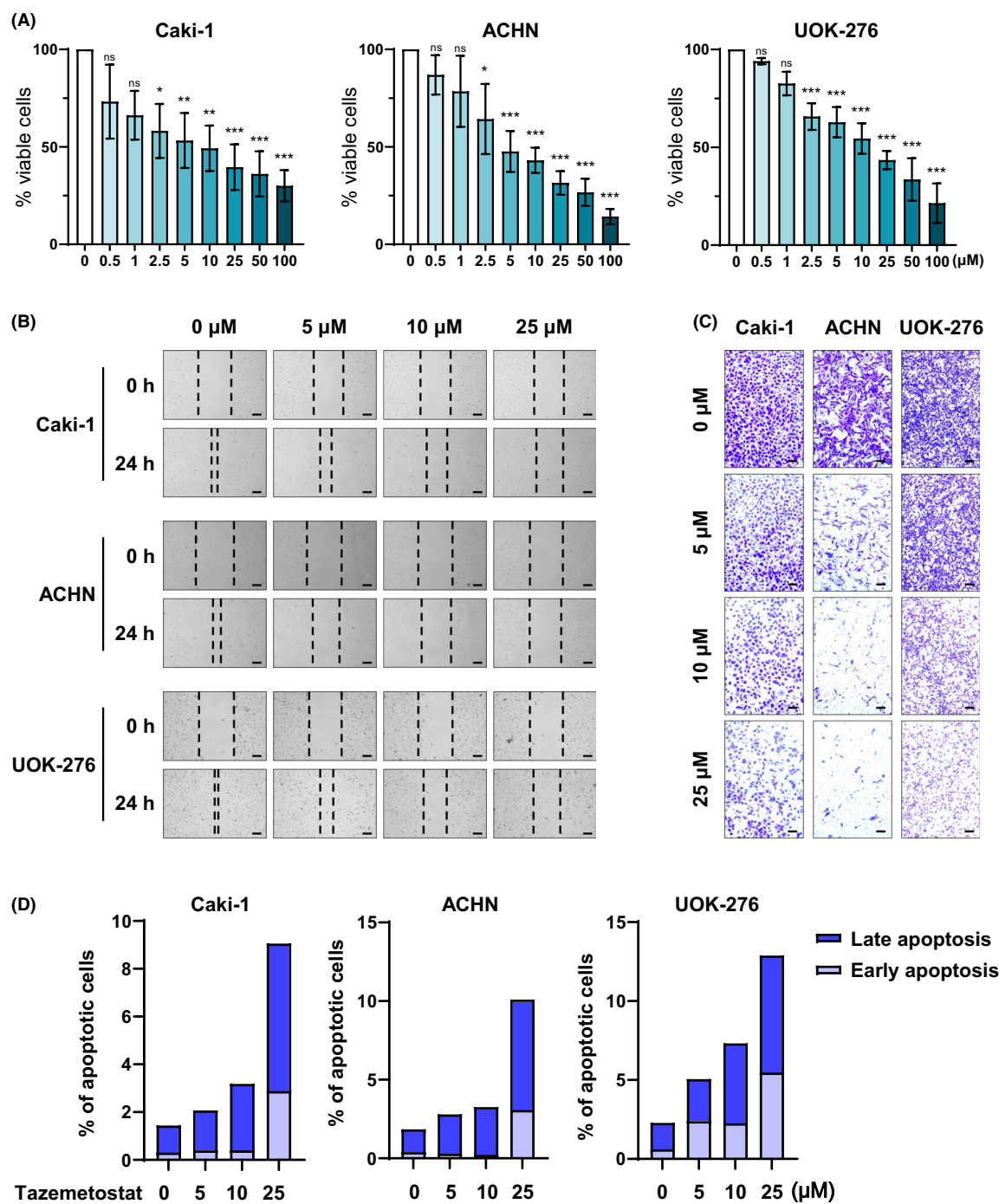


Fig. 1. Overexpressed *EZH2* inhibition induces antitumor effect in RCC. (A) Cell viability rate in Caki-1, ACHN, and UOK-276 cells with or without tazemetostat treatment (mean \pm SD, statistical calculations and comparisons were completed using a one-way analysis of variance and Tukey's *post hoc* test. $N = 3$; * $P < 0.05$, ** $P < 0.01$, *** $P < 0.001$). (B) Wound healing capacity determined for 24 h after tazemetostat treatment in Caki-1, ACHN, and UOK-276 cells (scale bars = 250 μ m). (C) Representative images of invaded cells that passed through transwell chambers in invasion assays using matrigel (0.4% crystal violet staining, 40 \times magnification; scale bars = 250 μ m). (D) Percentage of apoptotic cells based on annexin V-FITC/PI staining assay, and representative images for fluorescence-activated single cell sorting analysis performed after tazemetostat treatment in Caki-1, ACHN, and UOK-276 cells.

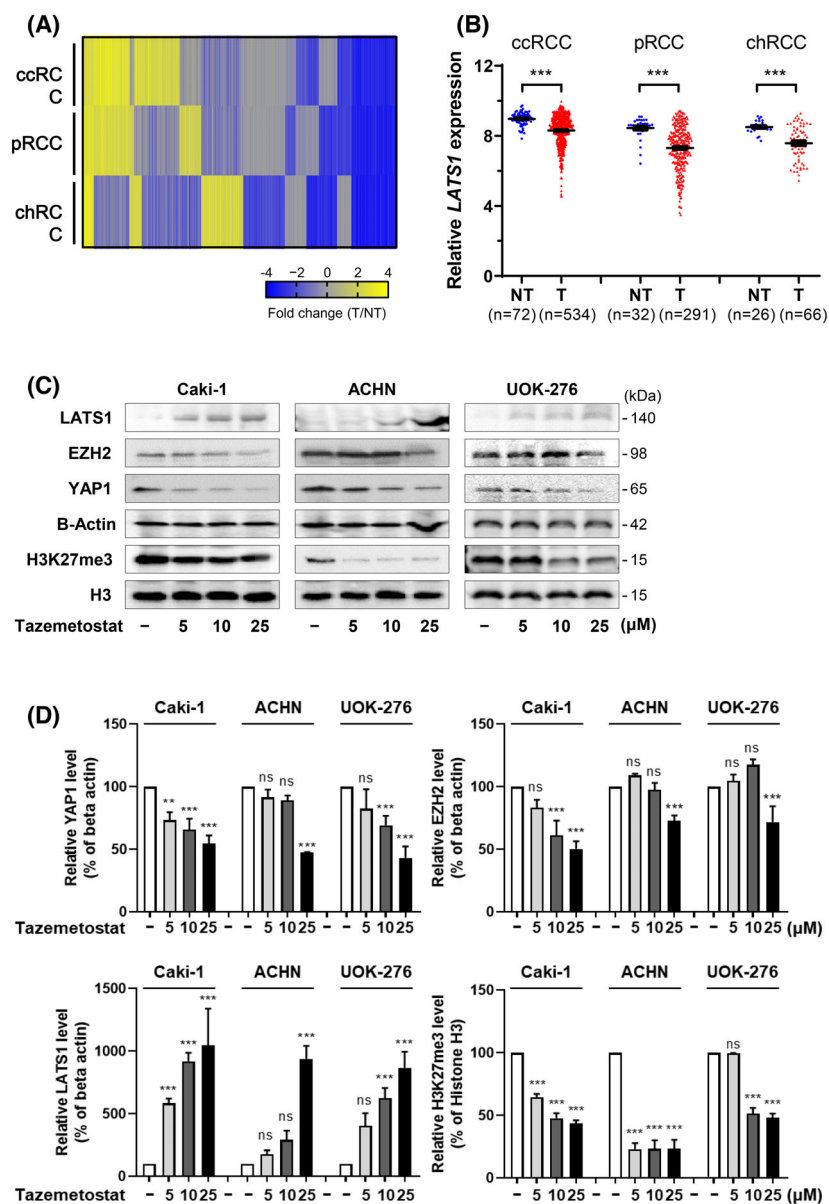


Fig. 2. *LATS1* of the Hippo pathway is the main target of EZH2 inhibition in RCC. (A) Significant downregulation of genes (n = 1850) in tumor compared with nontumor tissues in three types of RCC from the TCGA database. (B) Significant downregulation of *LATS1* expression in tissues of patients with RCC (ccRCC, pRCC, and chromophobe; chRCC) from the TCGA database (mean \pm SD, statistical calculations and comparisons were completed using a *t*-test) [****P* < 0.001, tumor (T) versus nontumor (NT) tissue]. (C, D) The protein levels of *LATS1*, *EZH2*, *YAP1*, and *H3K27me3* detected by western blot in RCC cell lines. As a loading control, beta-actin and histone H3 were used (mean \pm SD, statistical calculations and comparisons were completed using a one-way analysis of variance and Tukey's *post hoc* test. *N* = 3) (***P* < 0.01, ****P* < 0.001).

increased *LATS1* expression was evident after tazemetostat treatment (control, tazemetostat, si*LATS1*, tazemetostat + si*LATS1*: 100, 142.9, 6.1, and 8.5% for Caki-1; 100, 124.8, 6.8 and 8.5% for ACHN; and 100, 139.9, 23 and 114.9% for UOK-276, respectively). Furthermore, *LATS1* loss recovered the antitumorigenic effect of tazemetostat including reduced wound healing capability and invasion ability (control, tazemetostat, si*LATS1*, tazemetostat + si*LATS1*: 43.4, 74.1, 29.7, and 57.1% for Caki-1; 33.1, 84, 19.9 and 36.3% for ACHN; and 18.9, 71.9, 4.7 and 38.8% for UOK-276, respectively) (Fig. 3B,C and Fig. S3C). Increased RCC apoptosis by tazemetostat was rescued by inhibition of *LATS1* (control, tazemetostat,

si*LATS1*, tazemetostat + si*LATS1*: 2.8, 10.8, 1.9, and 3.5% for Caki-1; 2.2, 8.3, 1.4, and 2.4% for ACHN; and 4.3, 16.6, 1.1, and 12.7% for UOK-276, respectively) (Fig. 3D and Fig. S3D). Overall, the results indicate that *LATS1* is a direct target of the epigenetic regulator *EZH2* in three types of RCC cells.

Tazemetostat downregulates *LATS1* directly via suppression of *EZH2* binding at the *LATS1* promoter

To examine whether the upregulation of *LATS1* by tazemetostat is a result of direct regulation by inhibiting catalyation for *H3K27me3* on the *LATS1*

promoter, we performed ChIP using EZH2 and H3K27me3 antibodies (Fig. 4A). EZH2 was highly enriched at the promoter of *LATS1* in three cell lines, and it decreased upon treatment (24 h) with tazemetostat (tazemetostat treatment: 48.0 in Caki-1; 9.7% in ACHN; and 30.5% in UOK-276, respectively) (Fig. 4B). To delineate the epigenetic role of the *LATS1* promoter after tazemetostat treatment, ChIP was performed using H3K27me3 antibody, a well-known suppressive promoter marker. *LATS1* promoter regions were hypomethylated by EZH2 inactivation (tazemetostat treatment: 29.5 in Caki-1; 35.6% in ACHN; and 13.5% in UOK-276, respectively) (Fig. 4C), which corresponded with *LATS1* expression state (Fig. 2C). These results indicate that the epigenetic component EZH2 was correlated with *LATS1* transcription and *LATS1* is a direct target of EZH2 in RCC cells.

High EZH2 and low LATS1 expression are associated with poor outcomes in RCC patients

To verify the association between EZH2 and *LATS1* expression, immunohistochemistry (IHC) was performed using tissue from RCC patients. These IHC data showed that EZH2 is more highly expressed and *LATS1* is more lowly expressed in human RCC tissues than healthy tissues (NT/T: 1.7/25.9 for EZH2 and 10.3/2.2 for *LATS1*) (Fig. 5A,B). Furthermore, to verify the association between EZH2 and *LATS1* expression with public big data, we analyzed clinicopathological parameters based on TCGA cohort (mRNA) and TNM stage for ccRCC, pRCC, and chRCC. Among all samples from the TCGA cohort, some cases were missing part of the clinicopathological data. The median value for mRNA expression of *EZH2* and *LATS1* among all samples was chosen as a cutoff to classify the samples into high- and low-expression groups. We noticed that in the TCGA cohort, tumors of the high *EZH2* expression group were positively associated with stage IV in ccRCC (stage I, 40.78%; stage IV; 22.35%), pRCC (stage I, 63.89%; stage IV; 1.39%), and chRCC (stage I, 27.27%; stage IV; 6.06%) (Fig. 5C). However, the percentage of the high *LATS1* expression group was negatively associated with stage IV in ccRCC (stage I, 53.73%; stage IV; 12.94%), pRCC (stage I, 68.06%; stage IV; 0.69%), and chRCC (stage I, 39.39%; stage IV; 0%) (Fig. 5D). Although the ratios of stages according to the expression of *LATS1* in pRCC do not appear to be different on the graph, the ratios between the high *LATS1* expression group (stage I/II; 79.17%, stage III/IV; 20.83%) and the low *LATS1*

expression group (stage I/II; 78.62%, stage III/IV; 21.38%) are slightly different.

Discussion

We investigated the activity of an EZH2 inhibitor in RCC. Our findings revealed *LATS1* and Hippo pathway regulation as major targets of EZH2 inhibition (Fig. 6). This study found that EZH2 is overexpressed in RCC tissues compared with healthy tissues in three large cohorts, as well as in RCC cell lines. EZH2 inhibition by tazemetostat induced antitumorigenic effects including increased apoptosis, reduced wound healing capacity, and inhibition of invasive ability in RCC cell lines. The results of ChIP assays with antibodies against EZH2 and H3K27me3 and loss-of-function experiments against *LATS1* indicate that EZH2 directly modulates the transcription of *LATS1*. In contrast to EZH2, *LATS1* expression was downregulated in three large cohorts of RCC patients, suggesting that *LATS1* is a direct target of EZH2. Lastly, EZH2 expression was significantly associated with a higher stage of RCC, indicating that the EZH2-*LATS1* axis is an important target in patients with RCCs. Taken together, this study demonstrated that targeting epigenetic enzymes with EZH2 inhibitors will be an innovative therapeutic target for *LATS1*-underexpressed patients with RCC.

As the name suggests, ccRCC is characterized by cells with histologically empty cytoplasm because lipids and glycogen accumulated in the cell are removed during the histological process [24]. The study by Tun *et al.* [25] revealed that adipogenic genes change when renal epithelial cells are converted into tumors. Although lipid reprogramming in ccRCC is a well-known phenomenon, the importance of this process is still unclear. It is known that the Hippo pathway not only regulates the oncogene by translocation of YAP1 to the nucleus but also has complex regulatory functions related to the metabolism of various types of energy such as glucose [26–29] and lipids [30]. Although this study did not assess downstream genes of the Hippo pathway, this would be an important avenue for future study to determine how the EZH2-regulated Hippo pathway regulates metabolism given its crucial role in energy metabolism in RCC. In addition, ccRCC is sensitive to changes in glucose or lipid metabolism, whereas pRCC or chRCC can be controlled by other pathways, so further study is necessary. Because we used the TCGA database for the three types of RCC in our gene candidate discovery process, our study is not limited to ccRCC, which is a limitation of existing RCC treatment. Therefore, our

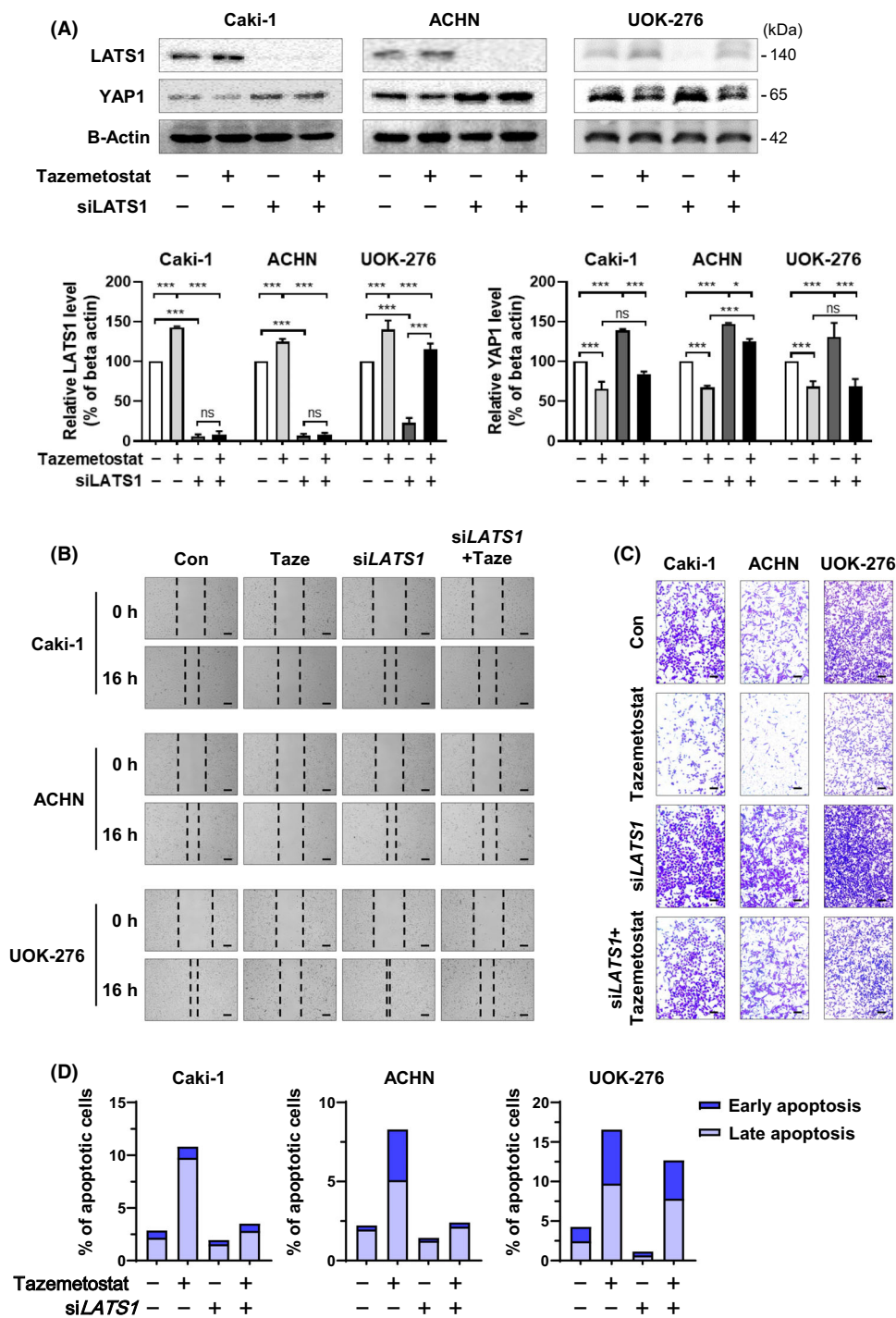


Fig. 3. Loss of LATS1 interferes with anticancer effects by EZH2 inactivation. (A) Endogenous protein expression levels of LATS1 and YAP1 were determined by western blot in RCC cell lines. As a loading control, beta-actin was used to quantify western blot data (mean \pm SD, statistical calculations and comparisons were completed using a one-way analysis of variance and Tukey's *post hoc* test. $N = 3$) ($*P < 0.05$, $***P < 0.001$). (B) Wound healing capacity determined for 16 h after treatment of 25 μ M tazemetostat and loss of LATS1 in Caki-1, ACHN, and UOK-276 cells (scale bars = 250 μ m). (C) Representative images of invaded cells that passed through transwell chambers in invasion assay using matrigel (0.4% crystal violet staining, 40 \times magnification) (scale bars = 250 μ m). (D) Annexin V-FITC/PI staining assay and the representative images for fluorescence-activated single cell sorting analysis performed after 25 μ M tazemetostat treatment and loss of LATS1 in Caki-1, ACHN, and UOK-276 cells.

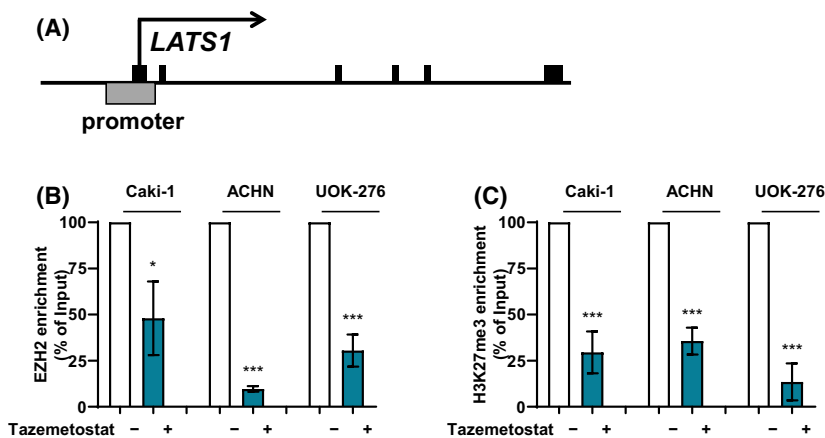


Fig. 4. Tazemetostat downregulates *LATS1* directly via suppression of EZH2 binding at the *LATS1* promoter. (A) Schematic diagram of the *LATS1* promoter. On the line, the black boxes indicate exon, and the gray box indicates the *LATS1* promoter region for a specific primer. Chromatin digested with enzymes was immunoprecipitated using anti-EZH2 and anti-H3K27me3 antibodies. (B, C) In the *LATS1* regulatory region, changes for the (B) binding of EZH2 and (C) enrichment of H3K27me3 by 25 μ M tazemetostat treatment based on qPCR analysis (mean \pm SD, statistical calculations and comparisons were completed using a one-way analysis of variance and Tukey's *post hoc* test. $N = 3$) (* $P < 0.05$, *** $P < 0.001$).

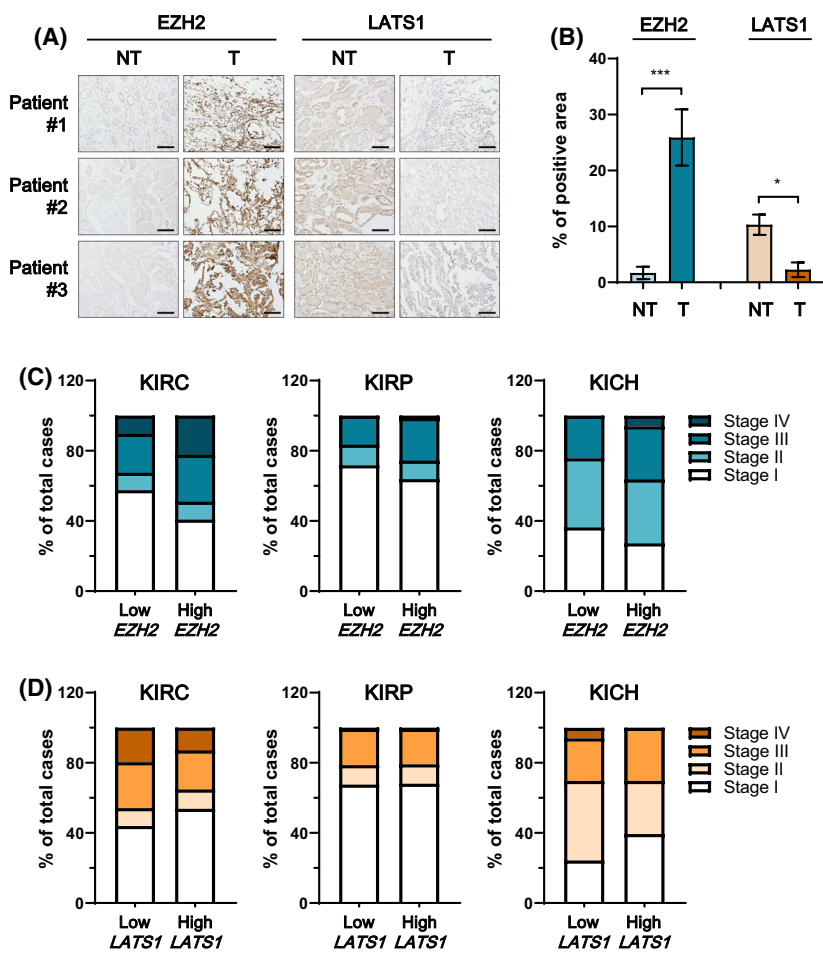


Fig. 5. High *EZH2* and low *LATS1* expression are associated with poor outcomes in RCC patients. (A) Representative image showing immunohistochemical analysis for EZH2 and H3K27me3 antibodies in healthy and tumor tissues from three patients (scale bars = 100 μ m). (B) Percentage of positive area in tumor and nontumor tissues immunohistochemically stained with anti-EZH2 and anti-H3K27me3 antibodies analyzed using LAS version 4.1.0 software (mean \pm SD, statistical calculations and comparisons were completed using a one-way analysis of variance and Tukey's *post hoc* test. $N = 3$) (* $P < 0.05$, *** $P < 0.001$). (C, D) Distribution of the clinical stages relative to (C) *EZH2* and (D) *LATS1* mRNA expression in RCCs.

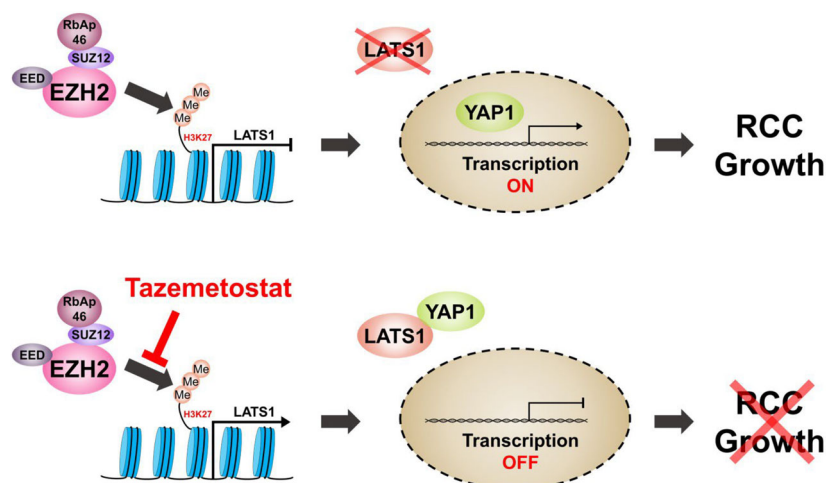


Fig. 6. Overexpressed EZH2 suppresses expression of LATS1 by inducing methylation in LATS1 promoter. Decreased LATS1 promotes the transcription of YAP1, a downstream gene, and induces RCC growth. However, the inactivation of EZH2 by tazemetostat inhibits RCC growth by blocking the methylation of LATS1 promoter.

results may provide the basis for studying how glucose or lipid metabolism is modulated in other RCCs.

In addition, tyrosine kinase inhibitors (TKIs), drugs widely used for the treatment of RCC, mainly inhibit angiogenesis [31], and complete tumor remission and sufficient survival gain are difficult to achieve with these drugs. In the case of sunitinib, a representative TKI, resistance has been noted as a problem for the last decade [32–34]. A recent study revealed that the mechanism for the acquisition of sunitinib resistance is closely associated with EZH2 [35]. Based on this research, the combination therapy of tazemetostat and the drugs currently used for RCC could be a new treatment strategy for RCC.

In several studies, the advantage of EZH2 as a target in cancer was reported, and especially, Nitya *et al.* reported that tazemetostat had the lowest *in vitro* IC50 as well as Methyl IC50 compared with GSK126 and CPI-1205 among EZH2 inhibitors currently in preclinical or early clinical trials [36,37]. Research is being conducted to show that tazemetostat is useful for combination therapy with many drugs in various cancers, and tazemetostat was suggested as a potential drug to be used in combination with immunotherapy such as pembrolizumab (NCT03854474). So, it is necessary to optimize the combination of tazemetostat with various drugs including TKI or immunotherapy. However, there is research that tazemetostat is an effective compound but not suitable for patients with renal injury [38]. So it is essential to check the renal injury and review the drug response before applying combination therapy or treatment using tazemetostat.

Taken together, we revealed that *EZH2* as an epigenetic enzyme is overexpressed in three types of RCCs. To our knowledge, this study is the first to demonstrate that an EZH2 inhibitor suppresses the inhibition of LATS1 transcription and its downstream pathway

in RCCs. In further studies, it would be intriguing to examine the intricate connection between tazemetostat and other drugs, which would undoubtedly shed light on the physiological significance for the treatment of various cancers due to the dysregulation of epigenetic components. Also, we expect these results to bring significant benefits for time and cost to the field and treatment for RCC patients.

Acknowledgements

This research was funded by the Basic Science Research Program through the National Research Foundation of Korea (NRF) funded by the Ministry of Education (grant number 2019M3E5D1A01069349 and 2020R1I1A1A01067390).

Author contributions

SHH and YEY involved in research conception and design. SHH and HJH involved in data acquisition. SHH and HJH involved in statistical analysis. SHH and YEY involved in data analysis and interpretation. SHH, SYP, and YEY involved in drafting of the manuscript. SHH and YEY involved in critical revision of the manuscript. HJH, DHS, and ESK involved in administrative, technical, or material support.

Conflict of interest

The authors declare no conflict of interest.

Data accessibility

The data presented in this study are available upon request from the corresponding author.

References

- Hyuna S, Jacques F, Rebecca LS, Mathieu L, Isabelle S, Ahmedin J and Freddie B (2021) Global cancer statistics 2020: GLOBOCAN estimates of incidence and mortality worldwide for 36 cancers in 185 countries. *CA Cancer J Clin* **71**, 209–249.
- Moch H (2013) An overview of renal cell cancer: pathology and genetics. *Semin Cancer Biol* **23**, 3–9.
- Yamaguchi H and Hung MC (2014) Regulation and role of EZH2 in cancer. *Cancer Res Treat* **46**, 209–222.
- Vire E, Brenner C, Deplus R, Blanchon L, Fraga M, Didelot C, Morey L, Van Eynde A, Bernard D and Vanderwinden JM (2006) The Polycomb group protein EZH2 directly controls DNA methylation. *Nature* **439**, 871–874.
- Cao R, Wang L, Wang H, Xia L, Erdjument-Bromage H, Tempst P, Jones RS and Zhang Y (2002) Role of histone H3 lysine 27 methylation in Polycomb-group silencing. *Science* **298**, 1039–1043.
- Yoo KH and Hennighausen L (2012) EZH2 methyltransferase and H3K27 methylation in breast cancer. *Int J Biol Sci* **8**, 59–65.
- Jin X, Kim LJY, Wu Q, Wallace LC, Prager BC, Sanvoranart T, Gimple RC, Wang X, Mack SC and Miller TE (2017) Targeting glioma stem cells through combined BMI1 and EZH2 inhibition. *Nat Med* **23**, 1352–1361.
- Arisan S, Buyuktuncer ED, Palavan-Unsal N, Caskurlu T, Cakir OO and Ergenekon E (2005) Increased expression of EZH2, a polycomb group protein, in bladder carcinoma. *Urol Int* **75**, 252–257.
- Chen S, Pu J, Bai J, Yin Y, Wu K, Wang J, Shuai X, Gao J, Tao K and Wang G (2018) EZH2 promotes hepatocellular carcinoma progression through modulating miR-22/galectin-9 axis. *J Exp Clin Cancer Res* **37**, 3.
- Wang X, Zhao H, Lv L, Bao L, Wang X and Han S (2016) Prognostic significance of EZH2 expression in non-small cell lung cancer: a meta-analysis. *Sci Rep* **6**, 19239.
- Frankel AE, Liu X and Minna JD (2016) Developing EZH2-targeted therapy for lung cancer. *Cancer Discov* **6**, 949–952.
- Zhou X, Zang X, Ponnusamy M, Masucci MV, Tolbert E, Gong R, Zhao TC, Liu N, Bayliss G, Dworkin LD *et al.* (2016) Enhancer of Zeste homolog 2 inhibition attenuates renal fibrosis by maintaining Smad7 and phosphatase and Tensin homolog expression. *J Am Soc Nephrol* **27**, 2092–2108.
- Ardestani A, Lupse B and Maedler K (2018) Hippo signaling: key emerging pathway in cellular and whole-body metabolism. *Trends Endocrinol Metab* **29**, 492–509.
- Meng Z, Moroishi T and Guan KL (2016) Mechanisms of Hippo pathway regulation. *Genes Dev* **30**, 1–17.
- Mo JS, Park HW and Guan KL (2014) The hippo signaling pathway in stem cell biology and cancer. *EMBO Rep* **15**, 642–656.
- Schneider CA, Rasband WS and Eliceiri KW (2012) NIH image to ImageJ: 25 years of image analysis. *Nat Methods* **7**, 671–675.
- Cancer Genome Atlas Research Network (2013) Comprehensive molecular characterization of clear cell renal cell carcinoma. *Nature* **449**, 43–49.
- Cancer Genome Atlas Research Network, Linehan WM, Spellman PT, Ricketts CJ, Creighton CJ, Fei SS, Davis C, Wheeler DA, Murray BA and Schmidt L (2016) Comprehensive molecular characterization of papillary renal-cell carcinoma. *N Engl J Med* **374**, 135–145.
- Davis CF, Ricketts CJ, Wang M, Yang L, Cherniack AD, Shen H, Buhay C, Kang H, Kim SC and Fahey CC (2014) The somatic genomic landscape of chromophobe renal cell carcinoma. *Cancer Cell* **26**, 319–330.
- Liberzon A, Birger C, Thorvaldsdóttir H, Ghandi M, Mesirov JP and Tamayo P (2015) The molecular signatures database (MSigDB) hallmark gene set collection. *Cell Syst* **6**, 417–425.
- Knutson SK, Kawano S, Minoshima Y, Warholic NM, Huang KC, Xiao Y, Kadowaki T, Uesugi M, Kuznetsov G and Kumar N (2014) Selective inhibition of EZH2 by EPZ-6438 leads to potent antitumor activity in EZH2-mutant non-Hodgkin lymphoma. *Mol Cancer Ther* **13**, 842–854.
- Wassef M, Michaud A and Margueron R (2016) Association between EZH2 expression, silencing of tumor suppressors and disease outcome in solid tumors. *Cell Cycle* **15**, 2256–2262.
- Ren G, Baritaki S, Marathe H, Feng J, Park S, Beach S, Bazeley PS, Beshir AB, Fenteany G and Mehra R (2012) Polycomb protein EZH2 regulates tumor invasion via the transcriptional repression of the metastasis suppressor RKIP in breast and prostate cancer. *Cancer Res* **72**, 3091–3104.
- Du W, Zhang L, Brett-Morris A, Aguila B, Kerner J, Hoppel CL, Puchowicz M, Serra D, Herrero L and Rini BI (2017) HIF drives lipid deposition and cancer in ccRCC via repression of fatty acid metabolism. *Nat Commun* **8**, 1769.
- Tun HW, Marlow LA, von Roemeling CA, Cooper SJ, Kreinest P, Wu K, Luxon BA, Sinha M, Anastasiadis PZ and Copland JA (2010) Pathway signature and cellular differentiation in clear cell renal cell carcinoma. *PLoS One* **5**, e10696.
- Enzo E, Santinon G, Pocaterra A, Aragona M, Bresolin S, Forcato M, Grifoni D, Pession A, Zanconato F and Guzzo G (2015) Aerobic glycolysis tunes YAP/TAZ transcriptional activity. *EMBO J* **34**, 1349–1370.
- DeRan M, Yang J, Shen CH, Peters EC, Fitamant J, Chan P, Hsieh M, Zhu S, Asara JM and Zheng B (2014) Energy stress regulates hippo-YAP signaling involving AMPK-mediated regulation of angiomin-like 1 protein. *Cell Rep* **9**, 495–503.

- 28 Wang W, Xiao ZD, Li X, Aziz KE, Gan B, Johnson RL and Chen J (2015) AMPK modulates Hippo pathway activity to regulate energy homeostasis. *Nat Cell Biol* **17**, 490–499.
- 29 Mo JS, Meng Z, Kim YC, Park HW, Hansen CG, Kim S, Lim DS and Guan KL (2015) Cellular energy stress induces AMPK-mediated regulation of YAP and the hippo pathway. *Nat Cell Biol* **17**, 500–510.
- 30 Santos CR and Schulze A (2012) Lipid metabolism in cancer. *FEBS J* **279**, 2610–2623.
- 31 Schoffski P, Dumez H, Clement P, Hoeben A, Prenen H, Wolter P, Joniau S, Roskams T and Van Poppel H (2006) Emerging role of tyrosine kinase inhibitors in the treatment of advanced renal cell cancer: a review. *Ann Oncol* **17**, 1185–1196.
- 32 Bhatt RS, Wang X, Zhang L, Collins MP, Signoretti S, Alsop DC, Goldberg SN, Atkins MB and Mier JW (2010) Renal cancer resistance to antiangiogenic therapy is delayed by restoration of angiostatic signaling. *Mol Cancer Ther* **9**, 2793–2802.
- 33 Morais C (2014) Sunitinib resistance in renal cell carcinoma. *J Kidney Cancer VHL* **1**, 1–11.
- 34 Makhov P, Joshi S, Ghatalia P, Kutikov A, Uzzo RG and Kolenko VM (2018) Resistance to systemic therapies in clear cell renal cell carcinoma: mechanisms and management strategies. *Mol Cancer Ther* **17**, 1355–1364.
- 35 Adelaiye-Ogala R, Budka J, Damayanti NP, Arrington J, Ferris M, Hsu CC, Chintala S, Orillion A, Miles KM and Shen L (2017) EZH2 modifies sunitinib resistance in renal cell carcinoma by kinome reprogramming. *Cancer Res* **77**, 6651–6666.
- 36 Kim KH and Roberts CW (2016) Targeting EZH2 in cancer. *Nat Med* **22**, 128–134.
- 37 Gulati N, Béguelin W and Giulino-Roth L (2018) Enhancer of zeste homolog 2 (EZH2) inhibitors. *Leuk Lymphoma* **59**, 1574–1585.
- 38 Li T, Yu C and Zhuang S (2021) Histone methyltransferase EZH2: a potential therapeutic target for kidney diseases. *Front Physiol* **12**, 640700.

Supporting information

Additional supporting information may be found online in the Supporting Information section at the end of the article.

Fig. S1. *EZH2* is overexpressed in renal cell carcinoma (RCC). (A) Analysis of gene family categorized to provide a functional overview for 156 genes with increased expression in tumor compared with nontumor tissues. (B) Significant overexpression of *EZH2* in the RCC tissues of three cohorts (ccRCC, pRCC, and chRCC) from the TCGA database (mean \pm SD, statistical calculations and comparisons were completed using a *t*-test) (***P* < 0.01 and ****P* < 0.001, versus nontumor tissue).

Fig. S2. Overexpressed EZH2 inhibition induces growth suppression in RCCs. (A) Annexin V–fluorescein isothiocyanate (FITC)/propidium iodide (PI) staining assay and the representative images for fluorescence-activated single cell sorting (FACS) analysis performed after tazemetostat treatment in Caki-1, ACHN, and UOK-276 cells. (B) The protein levels of LATS1, EZH2, YAP1, and H3K27me3 detected by western blot in HK-2 cell lines. As a loading control, beta-actin and histone H3 were used (mean \pm SD, statistical calculations and comparisons were completed using a one-way analysis of variance and Tukey's *post hoc* test. *N* = 3) (**P* < 0.05, ***P* < 0.01 and ****P* < 0.001).

Fig. S3. Loss of *LATS1* interferes with apoptosis by EZH2 inactivation. (A) *LATS1* mRNA levels determined by qRT-PCR after the loss of *LATS1* expression in Caki-1 cells. (B) Endogenous protein expression levels of LATS1 and YAP1 were determined by western blot in HK-2 cell lines. As a loading control, beta-actin was used to quantify western blot data. (C) Representative images for fluorescence-activated single cell sorting (FACS) analysis. Annexin V–fluorescein isothiocyanate (FITC)/propidium iodide (PI) staining assay was performed after tazemetostat treatment and loss of *LATS1* in Caki-1, ACHN, and UOK-276 cells (mean \pm SD, statistical calculations and comparisons were completed using a one-way analysis of variance and Tukey's *post hoc* test. *N* = 3) (**P* < 0.05, ***P* < 0.01 and ****P* < 0.001).